Journal of Chromatography A, 1217 (2010) 8167–8180

Contents lists available at ScienceDirect

Journal of Chromatography A

journal homepage: www.elsevier.com/locate/chroma

Mass transfer mechanism in liquid chromatography columns packed with shell particles: Would there be an optimum shell structure?

Fabrice Gritti, Georges Guiochon*

Department of Chemistry, University of Tennessee, Knoxville, TN 37996-1600, USA

ARTICLE INFO

Article history:
Received 12 July 2010
Received in revised form
14 September 2010
Accepted 18 October 2010
Available online 28 October 2010

Keywords:
Column packing technology
Mass transfer
Shell particles
Van Deemter curve
HETP
Halo-C_{18}
Kinetex-C_{18}
Pore size distribution

ABSTRACT

The mass transfer mechanisms in columns packed with old (55 μm Zipax and 5 μm Poroshell) and recently commercialized shell particles (2.7 μm Halo-C_{18} and Kinetex-C_{18}) were investigated from a *physico-chemical* point of view. Combining a model of diffusion in heterogeneous packed beds (effective medium theory) with values of the heights equivalent to a theoretical plate (HETPs derived from the first and second central moments of the elution profiles) and of the peak variances provided by the peak parking method, we demonstrate that columns packed with current shell particles perform better than those packed with fully porous particles in resolving low molecular weight compounds because the eddy diffusion term of the van Deemter equation of the former is markedly smaller. The calculation of eddy diffusion in column beds suggests that the smaller *A* terms are due to smaller trans-column velocity bias in columns packed with shell particles. We also show that the mass transfer of large molecules (e.g., proteins) is faster when the internal volume accessible to the analyte increases. Therefore, it is suggested that shell particles made of concentric layers with average pore sizes increasing with increasing diameter would provide columns with higher efficiency.

1. Introduction

Horváth et al. [1] conceived pellicular particles as packing materials for liquid chromatography in the late 1960s. They prepared 50 μm glass silica beads coated with a thin film of ion exchange resin and used columns packed with them to separate nucleotides, expecting two advantages: (1) a high loading capacity due to the large saturation capacity of the resin and (2) a low solid–liquid mass transfer resistance, due to the thin stationary phase layer [2,3]. In spite of the impressive separations reported by Horváth et al., this type of stationary phase was not adopted by the community because ion-exchange is a retention mechanism specific to ions, which did not interest much early chromatographers who preferred to develop liquid–liquid (LLC) rather than liquid–solid (LSC) chromatography, due to the poor results generally obtained in gas–solid chromatography. Huber [4,5], Halasz et al. [6], and Karger [7] pioneered LLC for a few years. This was why, 50 and later 35 μm shell particles were made, with a solid core of glass beads similar to the beads used by Horváth et al., surrounded by a ca. 1 μm thin layer of fine silica particles. This layer was impregnated with a liquid serving as the stationary phase. Several brands of these shell particles were commercialized in the early 1970s, including the 37–50 μm Corasil I and II (Waters Associates, 1970), the 50 μm Zipax (Dupont de Nemours, 1972), and the 50 μm Pellicosil (Macherey-Nagel, 1975) [8–10]. The volume fraction of the particle occupied by the porous shell was between 5 and 10% and the minimum reduced HETPs of the columns packed with them was between 2.0 and 2.5. However, it rapidly proved difficult to find two liquids practically insoluble in each other and between which the sample components would equilibrate with constants different from either zero or infinity. Furthermore, it was realized that LLC columns were unstable, rapidly losing stationary phase and providing irreproducible analyses. The use of liquid stationary phases was abandoned. Manufacturers of superficially porous packing materials tried to convert them to shell particles for LSC. However, the porous layers that had been designed to hold pools of the stationary liquid phase had a relatively small surface area, hence provided insufficient retention and a low loading capacity, becoming overloaded with very small size samples. In the same time, finer and finer fully porous particles were produced, permitting the production of more efficient columns and nullifying the potential advantages of the existing shell particles.

A second generation of shell particles appeared in 1992, with the 5 μm Poroshell (Agilent). It met only with limited success, in spite of allowing excellent separations [11]. Real success came

* Corresponding author at: Department of Chemistry, University of Tennessee, 552 Buehler Hall, Knoxville, TN 37996-1600, USA.
Tel.: +1 865 974 0733; fax: +1 865 974 2667.
E-mail addresses: guiochon@utk.edu, guiochon@ion.chem.utk.edu (G. Guiochon).

0021-9673/$ – see front matter © 2010 Elsevier B.V. All rights reserved.
doi:10.1016/j.chroma.2010.10.075

in 2006, with the introduction of the 2.7 μm Halo shell particles of Advanced Material Technologies[12,13]. The drawback of the low loading capacity of shell particles was eliminated by building a 0.5 μm thick porous shell around a 1.7 μm solid silica core. Therefore, the porous volume occupies about 75% of the particle volume. The most striking result was the achievement of 4.6 mm I.D. columns with a minimum reduced plate height of 1.5 for small molecules. This new packing material was designed for the separation of small molecular weight compounds [14]. Three years later, Phenomenex offered the 2.6 then the 1.7 μm Kinetex particles which exhibit exceptional performance, with a small h_{min} = 1.2 [15,16], a small C term [14,17], and a very flat HETP curve for both low and medium-size molecules. The C term results from the combination of two independent, additive mass transfer resistances. The first resistance accounts for the kinetics of diffusion of the sample molecules from the moving eluent (inter-particle volume) to the internal eluent (intra-particle volume), across the stagnant film of eluent surrounding the particles. The second mass transfer resistance term is due to the diffusivity of the sample across the particles, including the contributions of mesopore and surface diffusion. Early this year, Agilent came up with the new 2.7 μm Poroshell 120 while Advanced Material Technologies launched a second brand, the 2.7 μm Halo-ES-peptide shell particles [18] providing exceptional performance for peptides and small proteins. Packed in 4.6 mm I.D. tubes, all these particles give columns exhibiting plate heights equivalent to those achieved with the latest state-of-the-art sub-2 μm particles, with H between 3 and 4 μm.

We report here on the results of physico-chemical investigations of the reasons why 4.6 mm I.D. columns packed with modern shell particles perform so much better than fully porous particles. The analysis of the longitudinal diffusion coefficient (B coefficient) of the HETP equation was performed by applying the peak parking method to columns packed with fully and superficially porous particles [19–21]. The trans-particle mass transfer resistance coefficient (C_p coefficient) was determined by analyzing the results of peak parking measurements with a combination of several models of diffusion in heterogeneous packed beds and the general expression of C_p for mass transfer in porous media [2,3]. The external film mass transfer coefficient, C_f, was derived from the Wilson & Geankoplis correlation for small molecules [22]. This correlation was recently validated for the transfer of small molecules through porous particles [23]. The eddy diffusion term, A, was derived by subtraction of the $\frac{B}{\nu}$, $C_p\nu$, and $C_f\nu$ terms from the experimental reduced HETPs. Finally, we discuss the possibilities of improving the performance of these shell particles toward the separation of large molecules.

2. Theory

The overall reduced HETP of a chromatographic column can be accounted for as the sum of five main independent contributions that can be measured separately [21]: (1) longitudinal diffusion (the B term); (2) eddy diffusion (the A term); (3) the external film mass transfer resistance (the C_f term); (4) the trans-particle mass transfer resistance (the C_p term); and (5) an additional contribution due to the heat friction of the eluent percolating across the bed, the h_{Heat} term [24–27].

$$h = \frac{B}{\nu} + A(\nu) + C_f\nu + C_p\nu + h_{Heat} \quad (1)$$

The term h_{Heat} is negligible at small flow rates, for weakly adsorbed compounds and eluents having high thermal conductivities or under adiabatic conditions [28].

The reduced interstitial velocity ν and the reduced HETP are defined as

$$\nu = \frac{ud_p}{D_m} \qquad h = \frac{H}{d_p} \quad (2)$$

where H is the column HETP, d_p the average particle size of the packing material, D_m is the bulk molecular diffusivity, and u the interstitial linear velocity given by:

$$u = \frac{F_v}{\epsilon_e \pi R_c^2} \quad (3)$$

where F_v is the volume flow rate of the mobile phase, ϵ_e is the interstitial porosity, and R_c the inner radius of the column tube. The determination of the diffusion coefficients was explained elsewhere [21].

3. Experimental

3.1. Chemicals

The mobile phases were either mixtures of water and acetonitrile or pure tetrahydrofuran. Dichloromethane ($\rho_{CH_2Cl_2}$ = 1.323 g/cm^3) was used to measure the column hold-up volumes by pycnometry in combination with tetrahydrofuran (ρ_{THF} = 0.883 g/cm^3). These four solvents were HPLC grade from Fisher Scientific (Fair Lawn, NJ, USA). The mobile phase was filtered before use on a surfactant-free cellulose acetate filter membrane, 0.2 μm pore size (Suwannee, GA, USA). Insulin was a generous gift from Eli Lilly (Indianapolis, IN, USA). Trifluoro acetic acid (TFA), thiourea, and naphtho[2,3-a]pyrene were also purchased from Fisher Scientific. The sample test mixture containing uracil, acetophenone, toluene, and naphthalene in pure acetonitrile was generously offered by Phenomenex (Torrance, CA, USA).

3.2. Columns

The Kinetex 2.6 μm C_{18} 100 Å and Luna 3.0 μm C_{18}(2) 100 Å columns (100 mm × 4.6 mm) were offered by the manufacturer (Phenomenex, Torrance, CA, USA). The 2.7 μm Halo-C_{18} 90 Å and Halo-ES-peptide-C_{18} 160 Å columns (150 mm × 4.6 mm) were generous gifts from the column manufacturer (Advanced Material Technologies, Wilmington, DE, USA). The 1.7 μm BEH-C_{18} 135 Å and 300 Å (100 mm × 3.0 mm, 150 mm × 4.6 mm, and 50 mm × 2.1 mm) and 3.0 μm Atlantis-dC_{18} (150 mm × 4.6 mm) columns were also provided by the manufacturer (Waters, Mildford, MA, USA).

It is worth noting that, out of a lot of 133 columns packed with the same batch of Kinetex particles, following the same packing procedure, the efficiency of the best column deviated by less than 10% from the mean efficiency. The average particle size of Kinetex particles (2.5 μm) was measured by the Coulter counter technique after calibration of this instrument with the scanning electron microscopy (SEM) data obtained for the same lot of particles.

3.3. Measurement of the HETP data

3.3.1. Low molecular weight compounds: uracil, acetophenone, toluene, and naphthalene

The mobile phase was a mixture of water and acetonitrile (20/80, v/v). The sample volume injected was 1 μL. Although it is theoretically possible that a mismatch between the composition of the eluent (80% ACN) and that of the sample solution (100% ACN) affects somewhat the evaluation of the mass transfer kinetics parameters, in practice it would be difficult to detect the influence of the injection of a 1 μL sample on the efficiency of a 100 mm × 4.6 mm

column. The sample concentration was kept low in order to operate in the linear range of the adsorption isotherm while keeping an acceptable signal level. An experimental test was carried out by injecting successively 1, 2, and 5 μL samples. The amount injected was considered low enough if, after normalization of all three chromatograms, the peak shapes were not distorted by either non-linear adsorption behavior or non-linear detection response. The detection wavelength was set at 254 nm. The bandwidth was fixed at 4 nm. In the presence of the column, the sampling rate was adjusted from 10 Hz (at very low flow rates) to 80 Hz (at high flow rates). In the absence of column (for the measurements of the extra-column contribution), the sampling rate was constant at 160 Hz. In all cases, the peaks were represented by at least 50 data points, e.g., the peak standard deviation was represented by at least 12 data points.

The sequence of flow rates was 0.05, 0.10, 0.20, 0.30, 0.40, 0.60, 0.80, 1.00, 1.20, 1.40, 1.60, 1.80, 2.00, 2.30, 2.60, 2.90, 3.20, and 3.50 mL/min.

All the measurements were carried out on a 1290 Infinity instrument (Agilent, Palo Alto, CA). All experimental HETP data reported in this work were corrected for the contributions of the instrument to the retention volume and the band broadening of the probe compounds. These contributions were measured by replacing the chromatographic column with a zero volume union connector. Because the contribution of the extra-column volume to band broadening is very sensitive to the nature of the eluent, through its viscosity and diffusion coefficient [29], these contributions were always measured at the same flow rate and with the same mobile phase and compound as those used to measure the variance of the eluted bands. The extra-column band variance was measured according to the full integration of the best analytical fit of a Gaussian-Exponentially Modified function (with 5 parameters) to the experimental band profile. Similarly, for the sake of data accuracy, the corrected h data were systematically determined by applying the integration method to the determination of the first (μ_1 and $\mu_{1,ex}$) and second central (μ'_2 and $\mu'_{2,ex}$) moments:

$$\mu_1 = \frac{\int_0^\infty C(t)t\,dt}{\int_0^\infty C(t)\,dt} \tag{4}$$

$$\mu'_2 = \frac{\int_0^\infty C(t)(t-\mu_1)^2\,dt}{\int_0^\infty C(t)\,dt} \tag{5}$$

The reduced column HETP h is then determined using the following definition:

$$h = \frac{L}{d_p}\frac{\mu'_2 - \mu'_{2,ex}}{(\mu_1 - \mu_{1,ex})^2} \tag{6}$$

where L is the column length.

The precision of the h data is given by

$$\left|\frac{\Delta h}{h}\right| = \left|\frac{\Delta\mu'_2}{\mu'_2}\right|\left(\frac{\mu'_2+\mu'_{2,ex}}{\mu'_2-\mu'_{2,ex}}\right) + 2\left|\frac{\Delta\mu_1}{\mu_1}\right|\left(\frac{\mu_1+\mu_{1,ex}}{\mu_1-\mu_{1,ex}}\right) \tag{7}$$

The moments of the peaks, μ_1 and μ'_2, were measured in triplicate, first with the chromatographic column fitted to the instrument, then after replacing the column with a zero-volume connector. The relative errors made on the second and first moments were always smaller than 5 and 0.5%, respectively. Accordingly, the error made increases with decreasing solute retention, e.g., when the terms between parentheses in the right-hand-side term of Eq. (7) becomes significantly larger than one.

3.3.2. Thiourea

The same method as described above for low molecular weight compounds was applied, except that the eluent was pure water.

3.3.3. Naphtho[2,3-a]pyrene

The same method as described above for small molecules was applied, except for the eluent composition (pure acetonitrile).

3.3.4. Insulin

The same method as described above for small molecules was applied, except that the eluent composition was a water–acetonitrile mixture (31/69, v/v) containing 0.1% TFA.

3.4. Peak parking measurements

The principle of this method was described earlier [19]. The flow rate was fixed at 0.4 mL/min for the low molecular weight compounds (thiourea, uracil, acetophenone, toluene, naphthalene, and naphtho[2,3-a]pyrene) and at 0.1 mL/min for the larger insulin.

4. Results and discussion

We first discuss the evolution of the performance of columns packed with shell particles since the early 1970s and analyze, from a theoretical point of view, the potential advantages of using shell particles rather than fully porous particles. In a second part, we compare the experimental and theoretical reduced HETPs and investigate why the performance of columns packed with shell particles is better than what should be anticipated from theory. Finally, we discuss what changes could be made to the design of shell particles to improve their performance in liquid chromatography.

4.1. Evolution of the performance of columns packed with shell particles

We measured the flow rate dependence of the reduced plate heights of naphtho[2,3-a]pyrene on four columns packed with shell particles using pure acetonitrile as the mobile phase.

1. The 4.6 mm × 300 mm column packed with 55 μm Zipax-C_{18} that was commercialized in 1972 by Dupont de Nemours (Wilmington, DE); these particles were made of a 50 μm non-porous glass core coated with a 5 μm thick layer of spherical 0.2 μm nano silica particles, giving a ratio $\rho = (d_c/d_p) = 0.90$, with d_c, the core diameter.
2. The 2.1 mm × 75 mm column packed with 5 μm Poroshell-C_{18}, introduced in 1992 by Hewlett-Packard (now Agilent Technologies, Palo Alto, CA); these particles have a shell thickness of 0.25 μm, with $\rho = 0.95$.
3. The 4.6 mm × 150 mm column packed with the first generation of 2.7 μm Halo-C_{18} particles (average pore size 90 Å), launched in 2006 by Advanced Material Technologies (Wilmington, DE); these particles have a 1.7 μm solid silica core and a 0.5 μm thick porous silica shell; and
4. The 4.6 mm × 100 mm column packed with 2.6 μm Kinetex-C_{18} produced by Phenomenex (Torrance, CA) in 2009; these particles have a 1.9 μm solid silica core covered with a 0.35 μm porous silica shell.

The performance of these columns will be compared to that of the 3.0 mm × 100 mm column packed with fully porous 1.7 μm BEH-C_{18} particles (Waters, Milford, MA).

Fig. 1A compares the reduced HETPs measured for the Zipax and the Poroshell columns. The plots of their reduced plate heights versus the reduced velocity near their minimum are similar between 2.0 and 2.5, corresponding to an optimal reduced velocity

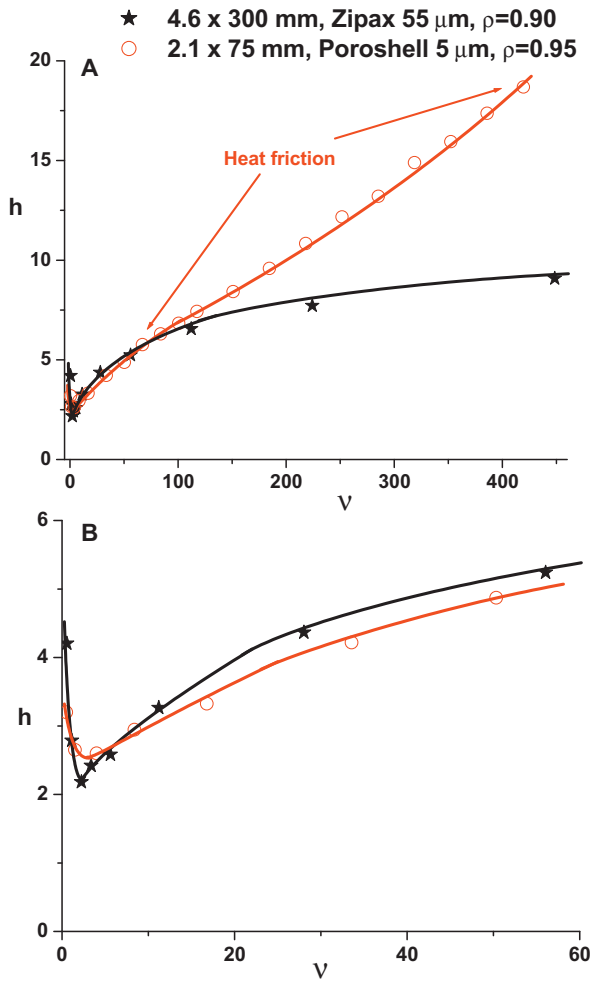

Fig. 1. Experimental reduced HETP plots of the old Zipax (1972) and Poroshell (1992) shell particles. (A) Full reduced linear velocity range $0 < \nu < 450$. (B) Zoom in for $\nu < 60$. Note the minimum reduced plate height in between 2.0 and 2.5.

of 2.5. Due to the differences in the column aspect ratios (2.1 mm *versus* 4.6 mm I.D.) and the particle sizes (5 μm *versus* 55 μm), the curve of the Poroshell column exhibits a serious efficiency loss due to friction heat generated inside the Poroshell column at high flow rates. For instance, at a reduced interstitial linear velocity of 100, the actual flow rate is 11 times faster through the Poroshell than through the Zipax column (1.2 mL/min *versus* 0.10 mL/min). The back pressure ΔP is about 200 bar for the 2.1 mm I.D. Poroshell column but is negligible for the Zipax column. Therefore, whereas the frictional heat generated in the Zipax column is negligible, it is significant in the Poroshell column and causes the formation of a significant radial gradient of temperature, even though this is a narrow bore column [28]:

$$P_f = F_\nu \times \frac{\Delta P}{L} \tag{8}$$

We estimate that the heat friction power in the 7.5 cm long Poroshell column is $((1.2 \times 10^{-6})/60) \times ((200 \times 10^5)/7.5 \times 10^{-2}) = 5.3$ W/m, a value larger than the critical threshold above which heat friction power begins to significantly affect column efficiency (4 W/m) [28]. This explains the convex downward shape of the reduced HETP curve of the Poroshell column at flow rates larger than 1.2 mL/min or $\nu > 100$. This results illustrates how the heat effect and its consequences do not depend on the column inlet pressure but on the product of the flow velocity and the pressure gradient [28].

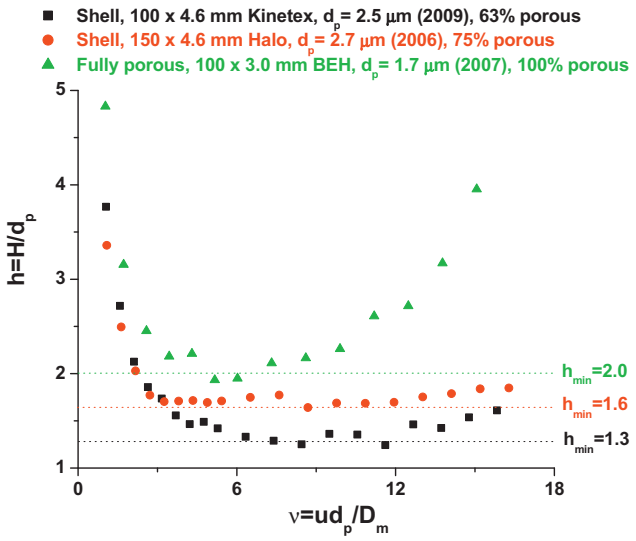

Fig. 2. Experimental reduced HETP plots of the new Halo (2006) and Kinetex (2009) shell particles. Comparison with the reduced plate height of a column packed with commercial sub-2 μm BEH particles. Note the comparable plate heights between shell and fully porous particles and the absence of the *C* term's uptake (due to heat friction) at high velocity with the shell particles.

Remarkably, for $\nu < 100$, the two HETP curves are very close (see Fig. 1B). The strong upward curvature suggests that the mass transfer of naphtho[2,3-a]pyrene is largely controlled by the eddy diffusion term (the reduced velocity for which the eddy diffusion term becomes equal to half its maximum limiting value, for $\nu \to \infty$, is around $\nu_{1/2} = 10$). Most likely, the packing quality of these two columns should be expected to be relatively poor, given the irregular shape of the Zipax particle and the small inner diameter of the Poroshell column (2.1 mm). Eventually, their minimum reduced HETP is not smaller than 2.0.

Fig. 2 shows the reduced HETPs of the Halo, Kinetex, and BEH columns. The considerable improvement in column performance brought about by shell particles is obvious. The minimum reduced plate height is only between 1.3 and 1.6 and the optimal reduced linear velocity reaches around 10. The HETP curve is nearly flat at high velocities, suggesting the absence of large scale trans-column velocity biases. Whereas the columns packed with the former superficially porous particles (Zipax and Poroshell) could not compete with those made of the smaller fully porous particles available at that time (10 μm in the 1970s and 3–3.5 μm in the 1990s) and could provide only relatively low loading capacities due to their large ρ values, today's columns packed of sub-3 μm shell particles provide the performance of sub-2 μm fully porous particles ($H_{min} \simeq 1.3 \times 2.5 \simeq 2.0 \times 1.7 \simeq 3.4$ μm) and a reasonable column loading capacity, due to the larger ratio of their shell thickness to the radius of their solid core, which accounts for about 70% of the particle volume. Actually, Fig. 2 shows a further advantage of using columns packed with shell particles at high flow rates: the efficiency loss due to friction heat is significant with sub-2 μm fully porous particles (hence the parabolic *C* branch observed) while it is marginal with columns packed with sub-3 μm shell particles (a nearly flat *C* branch is observed). This difference is explained by the lower pressure gradient (due to the larger particle size, ×1.5) and the higher heat conductivity of the packed beds (×2.5) due to the solid core of the shell particles [26].

The reasons for the exceptional performance of the new shell particles should be investigated in depth. For this purpose, we compare the experimental and theoretical (see next section) HETP curves of sub-3 μm shell and fully porous particles and determine the true origin for the high efficiency levels achieved

with columns packed with 2.7 μm Halo and 2.6 μm Kinetex particles.

4.2. Theoretical advantages of using shell particles

Due to the presence of the solid silica core of shell particles, the diffusion of sample molecules through these particles takes place only through the shell volume. Therefore, one can anticipate a decrease of the longitudinal diffusion coefficient (B coefficient) and a reduction of the trans-particle mass transfer coefficient (C_p coefficient). In the next two sub-sections, we analyze quantitatively the reduction of these two coefficients in the van Deemter equation.

4.2.1. Theoretical expressions of the B coefficient

A model of diffusion in heterogeneous packed beds is needed to estimate the value of the B term in packed beds, which should be considered as a heterogeneous binary mixture. The first homogeneous medium is the interstitial volume through which the eluent is moving, in which the diffusion coefficient is the molar diffusivity, with:

$$D_1 = D_m \tag{9}$$

The second homogeneous medium is the particle inner volume:

$$D_2 = D_p \tag{10}$$

where D_p is the effective diffusivity of the sample through the particle obtained by considering that the concentration gradient in the bulk is the driving force [30]. Additionally, we assume a volume average diffusivity in the particle volume and therefore D_p is written [14]:

$$D_p = \rho^3 \times 0 + (1-\rho^3)D_{eff} = (1-\rho^3)\Omega D_m \tag{11}$$

where Ω is the ratio of the sample diffusivity in the porous shell, D_{eff}, to the bulk molecular diffusion coefficient, D_m. Two different diffusion models are available.

4.2.1.1. Parallel diffusion model. The simplest diffusion model assumes that the diffusion fluxes in the interstitial volume and in the particle's volume are additive. The theoretical reduced B coefficient is then written [31] as a function of the structural parameter ρ:

$$B = 2\left[\gamma_e D_m + \frac{1-\epsilon_e}{\epsilon_e}(1-\rho^3)\Omega\right] \tag{12}$$

where γ_e is the external obstruction factor (0.6) and ϵ_e is the external porosity (0.4).

Fig. 3A illustrates how the B coefficient decreases from fully porous to shell particles in a real case, considering $\rho = 0.72$ (i.e., the case of 2.6 μm Kinetex particles with a shell thickness of 0.35 μm [14]), as a function of the coefficient Ω. This coefficient increases from 0.20 (non-retained sample) to 1.8 (retained samples), considering standard silica-C_{18} porous particles (100 Å, 250 m^2/g) in the RPLC mode [32]. Typically, for moderately retained compounds, Ω is close to unity. This would suggest that the B coefficient in the general reduced van Deemter equation (plotted as a function of the reduced interstitial linear velocity) decreases by −1.12.

4.2.1.2. Effective medium theory. This model is based on the general effective medium theory of Landauer [33], extended to molecular diffusion [34]. It was used to derive a rigorous expression of the B coefficient in packed chromatographic columns [31]:

$$B = \frac{2}{\epsilon_e}\left[a + \sqrt{a^2 + \frac{1}{2}(1-\rho^3)\Omega}\right] \tag{13}$$

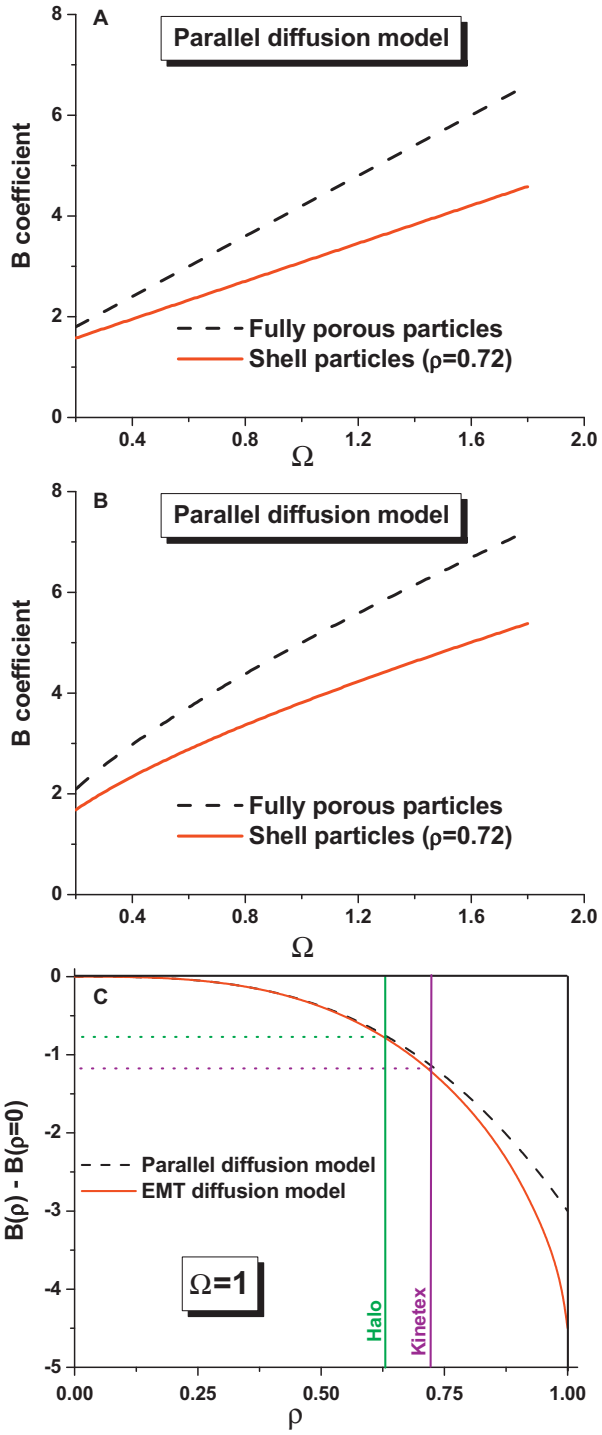

Fig. 3. Variation of the longitudinal diffusion coefficient, B, as a function of the ratio, Ω, of the sample diffusivity in the porous shell (D_{eff}) to the bulk molecular diffusion coefficient (D_m). (A) Parallel diffusion model Eq. (12). (B) Diffusion model derived from the effective medium theory (EMT) of Landauer equation (13). (C) Theoretical decrease of the B coefficient as a function of the particles' structural parameter, ρ, of the core diameter to the particle diameter. Note the similarity between the two models for $\rho < 0.75$.

with

$$a = \frac{1}{4}\left[3\epsilon_e - 1 + (2-3\epsilon_e)(1-\rho^3)\Omega\right] \tag{14}$$

Fig. 3B compares the theoretical B coefficients for columns packed with fully porous ($\rho = 0$) and with shell (with $\rho = 0.72$) particles calculated on the basis of the effective medium theory

of diffusion. Note that the shape of the curves is slightly convex upward instead of being strictly linear as with the results obtained in the previous section (see Fig. 3B). Although the two models are formally different, the second model predicts a decrease of the B coefficient for $\Omega = 1$ that is very close to the value predicted by the parallel diffusion model, e.g. −1.19 *versus* −1.12.

4.2.1.3. Value of the B term. Fig. 3C shows plots of the difference in the B term as a function of the ratio of the core to the particle diameters, between 0 (fully porous particles) and 1 (non-porous particles) and when $\Omega = 1$ (as for a moderately retained compound, with an equilibrium constant between the bulk eluent and the porous solid adsorbent $K_{shell} \simeq 4$). Remarkably, there is no significant difference between the decrease of the B coefficient predicted by either diffusion models for $\rho < 0.80$. In conclusion, both diffusion models predict the same decrease of the B coefficient for current commercial shell particles, including the 2.6 μm Kinetex ($\rho = 0.72$, $\Delta B = -1.15$) and the 2.7 μm Halo ($\rho = 0.63$, $\Delta B = -0.75$) particles. For instance, at a reduced linear velocity of $\nu = 8$, the longitudinal diffusion contribution to the reduced plate heights of the Halo and Kinetex columns decreases from $h = 0.58$ to 0.48 and from $h = 0.58$ to 0.44, respectively.

4.2.2. Theoretical expressions of the C_p coefficient

The solid silica core affects the rate at which the sample molecules diffuse through the particles. From a statistical point of view, the average residence time of a molecule inside a shell particle is smaller than that inside a fully porous particle having the same diameter, d_p. The C_p coefficient of columns packed with shell particles should be smaller than that of columns packed with fully porous particles. Using different approaches, Horváth and Lipsky [2] and, later, Kaczmarski and Guiochon [3] derived the rigorous expression of the C_p coefficient for shell particles:

$$C_p = \frac{1}{30}\frac{\epsilon_e}{1-\epsilon_e}\left[\frac{k_1}{1+k_1}\right]^2 \frac{1+2\rho+3\rho^2-\rho^3-5\rho^4}{\left(1+\rho+\rho^2\right)^2}\frac{1}{\Omega} \quad (15)$$

The results of both derivations show that the ratio of the C_p coefficients of the columns packed with shell and fully porous particles is [14]:

$$\frac{C_{p,shell}}{C_{p,fully\ porous}} = \left[\frac{1+k_1-\rho^3}{1+k_1}\right]^2 \frac{1+2\rho+3\rho^2-\rho^3-5\rho^4}{\left(1+\rho+\rho^2\right)^2} \quad (16)$$

where k_1 is the zone retention factor [3]:

$$k_1 = \frac{1-\epsilon_e}{\epsilon_e}\left[\epsilon_{shell,p} + (1-\epsilon_{shell,p})K_{shell}\right](1-\rho^3) \quad (17)$$

where K_{shell} is the Henry constant for the adsorption–desorption equilibrium of the solute in the porous adsorbent and $\epsilon_{p,shell}$ is the porosity of the shell (0.4).

Fig. 4A shows the variation of the ratio ($C_{p,shell}/C_{p,fully\ porous}$) with the Henry constant, K_{shell}, for a constant value of $\rho = 0.72$. We observe only a weak dependence of this ratio on the adsorption strength of the compound. At the limit, when $K_{shell} \to \infty$, the trans-particle mass transfer coefficient of the column packed with shell particle is 45% that of the column packed with fully porous particles. Fig. 4B shows the variation of the ratio of the C_p coefficients as a function of ρ for the Henry constant $K_{shell} \to \infty$. Typically, theory predicts that C_p is approximately twice smaller for the Halo (−42%) and the Kinetex (−55%) columns than for a column packed with fully porous particles.

It is interesting to compare the decrease of the $C_p\nu$ term when ρ increases and that of the longitudinal diffusion term at $\nu = 8$, close to the minimum of the HETP curves (see experimental data later), for $K_{shell} = 4$ and for $\Omega = 1$ (values corresponding to a moderately retained compound). This term decreases from 0.10 to 0.06 and from 0.09 to 0.04 for the Halo and the Kinetex columns, respectively. Despite a larger relative decrease of the $C_p\nu$ term (−50%), the effect on the reduced HETP values remain small compared to that of the longitudinal diffusion term (the relative decrease of which is only −25%).

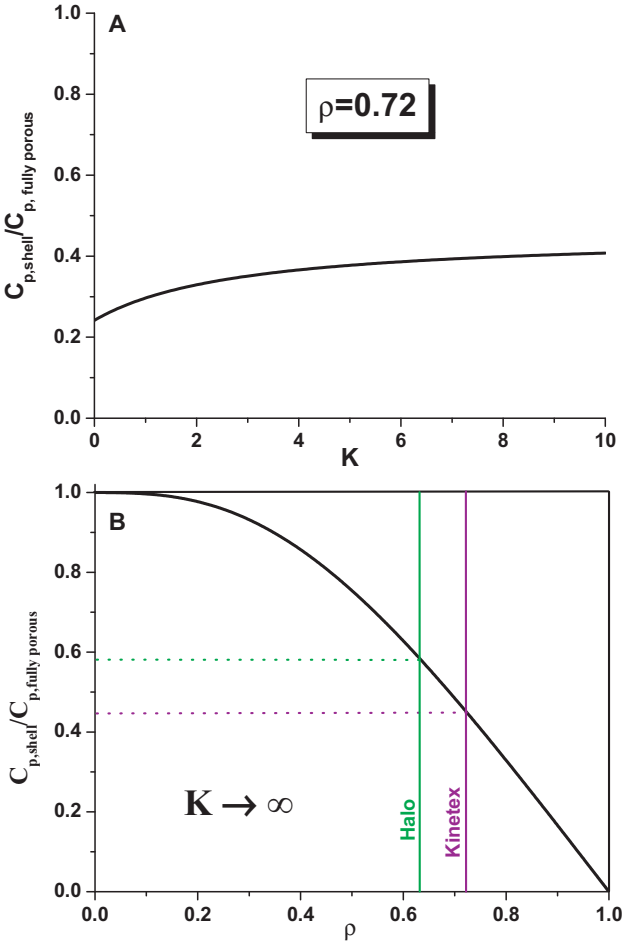

Fig. 4. Analysis of the theoretical trans-particle mass transfer coefficient, C_p, for shell and fully porous particles. (A) Ratio of the C_p coefficient of shell particles to that of fully porous particles as a function of the Henry's constant, K_{shell}. (B) Same as in Fig. 2A, except the x-axis is scaling the parameter ρ.

4.2.3. Theoretical values of the reduced HETPs

Assume two columns of identical dimensions, packed one with fully porous particles, the other with particles of the same sizes, and located in the same position, made with the same porous medium but having a solid core. The structural parameter, ρ, is constant throughout the bed. Therefore, we can assume that (1) the eddy diffusion terms, h_{eddy}, of the two columns are the same and (2) that the external film mass transfer coefficients, k_f, are also equal, the latter being given by the Wilson & Geankoplis correlation [22], which was validated recently with large and porous particles [23]. Therefore, the external film mass transfer can be written [35]:

$$h_{film} = \frac{1}{3}\frac{\epsilon_e}{1-\epsilon_e}\left[\frac{k_1}{1+k_1}\right]^2 \frac{1}{Sh} \quad (18)$$

The longitudinal diffusion term is calculated according to the EMT diffusion model (Eq. (13)) for $\Omega = 1$. The trans-particle mass transfer resistance term is obtained from Eq. (15). Finally, we simplify the

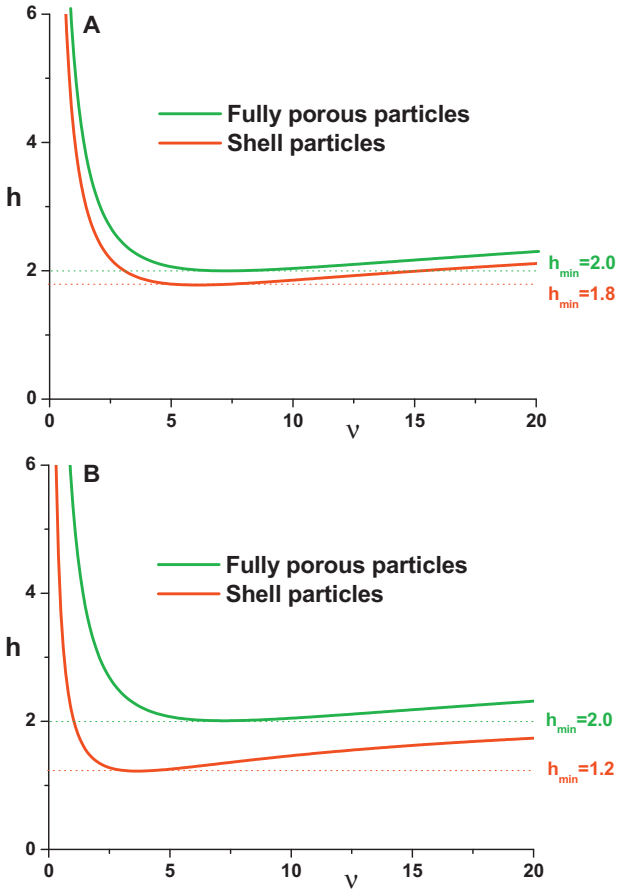

Fig. 5. Theoretical reduced HETP plots for fully and shell particles. (A) ρ=0.72 (Kinetex). (B) ρ = 0.95 (Zipax, Poroshell).

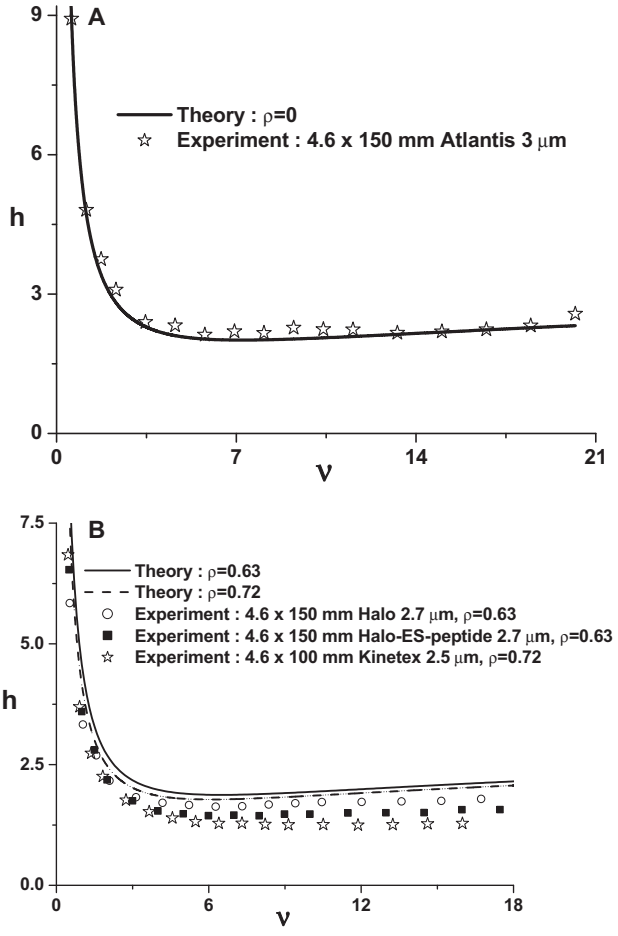

Fig. 6. Comparison between the theoretical and experimental reduced HETP plots. (A) Fully porous particles. Note the excellent agreement. (B) Shell particles. Note the systematic lower than expected experimental HETP assuming that columns packed with either fully or superficially porous particles have the same eddy diffusion *A* term.

eddy diffusion term by writing it as:

$$h_{eddy} = \frac{1}{(1/2\lambda) + (1/\omega\nu)} \tag{19}$$

The parameters λ and ω were selected as 1.1 and 0.28, respectively, giving a minimum reduced HETP of 2.0 and an optimal reduced linear velocity of 7, values which are typical of columns packed with fully porous particles. According to the theory, the minimum reduced HETP of the column packed with the shell particles is 1.8 (Fig. 5A), only 10% lower when the ratio ρ of the diameters of the core and the particle is equal to 0.72. When the same ratio is equal to 0.95 (which is the case for the earlier shell particles such as the 55 μm Zipax and the 5 μm Poroshell), the minimum reduced plate height would be expected to be as low as 1.2 (Fig. 5B) with an optimal reduced velocity shifting to smaller values ($\nu_{opt} \simeq 3.5$).

4.3. Comparison between experimental and calculated HETP values

Fig. 6 compares the theoretical (see above) and experimental HETPs of a retained compound (acetophenone, $K_{shell} \simeq 4$) on columns packed with fully porous and shell particles. Fig. 6A shows an excellent agreement between the experimental data recorded with the 4.6 mm × 150 mm column packed with 3 μm fully porous Atlantis particles. The fully porous 3.0 μm Atlantis particles were chosen because their average size was the closest to that of the 2.6 μm Kinetex and 2.7 μm Halo core–shell particles. In contrast, Fig. 6B demonstrates that the theoretical HETP derived for shell particles does not account satisfactorily for the experimental data collected with the 2.6 μm Kinetex (ρ = 0.72), the 2.7 μm Halo (ρ = 0.63), and the 2.7 μm Halo-ES-peptide (ρ = 0.63) particles. The experimental minimum reduced HETPs of these three columns are 1.25, 1.62, and 1.45, respectively, versus expected values of 1.78 (+42%), 1.87 (+15%), and 1.84 (+27%), respectively. These relative differences are significant and should be explained.

A first explanation could be that the decrease of the *B* coefficient was underestimated. This estimate is based on the diffusion models presented earlier. The peak parking technique permits to check this possible explanation. Measurements made for uracil, acetophenone, toluene, and naphthalene on all three columns give values of the longitudinal diffusion coefficient determined as follows:

$$B = \frac{1}{D_m} \frac{\Delta\sigma^2_{PP}}{\Delta t_p} \frac{u^2_{PP}}{1 + k_1} \tag{20}$$

where $(\Delta\sigma^2_{PP}/\Delta t_p)$ is the slope of the plot of the peak variance, σ^2_{PP}, measured in the peak parking method as a function of the parking time, t_p and u_{PP} is the interstitial linear flow velocity applied.

In order to compare the experimental and theoretical plots shown in Fig. 1B, we need to estimate the ratio Ω of the sample diffusivity in the porous shell, D_{eff}, to the bulk molecular diffusion coefficient, D_m, which was done using the axial diffusion model derived from the effective medium theory of Landauer [33] extended to mass diffusion [34] and to packed columns in LC [31]. Accordingly, Ω was numerically determined by solving the set of Eqs. (13), (14), and (20).

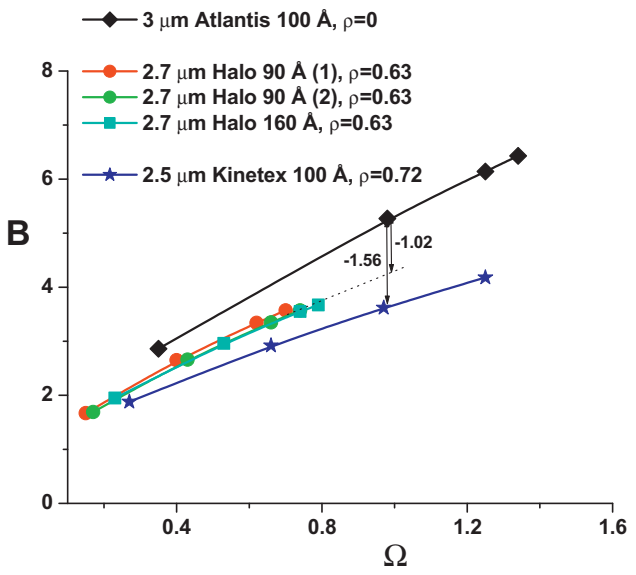

Fig. 7. Plots of the experimental longitudinal coefficient B (measured by the peak parking method) as a function of the parameter Ω (estimated from the peak parking method assuming the EMT diffusion model in the packed bed) for fully porous (Atlantis) and superficially porous (Halo, Kinetex) particles. First, note the continuous decrease of B as the parameter ρ increases. Second, note the slight convex upward shape of the plots.

The plots of the experimental values of B versus Ω are shown in Fig. 7 for the Atlantis ($\rho = 0$), two Halo 90 Å columns ($\rho = 0.63$, columns 1 and 2), the Halo 160 Å ($\rho = 0.63$), and the Kinetex 100 Å ($\rho = 0.72$) columns. The data show clearly that for $\Omega = 1$ the B coefficients of the Halo and the Kinetex columns are −1.02 and −1.56 smaller than that of the Atlantis column. The theory predicts a decrease of only −0.75 and −1.15, respectively. These values are in good qualitative agreement because the porous structures of all these particles are different.

These results demonstrate that the significant decrease in the minimum HETPs of the columns packed with shell particles at reduced interstitial linear velocities around $\nu = 10$ cannot be explained by the simple decrease of the B coefficient due to the presence of the solid silica core. This means that it was incorrect to assume earlier that the eddy diffusion coefficient, A, is the same for both types of columns, those packed with fully porous and with shell particles, in Eq. (19). This coefficient is definitely smaller for the columns of the latter type.

This conclusion is confirmed by the results of measurements of the eddy diffusion terms of these two types of columns.

4.4. Analysis of the eddy diffusion coefficient

The eddy diffusion terms were derived from the results of experimental measurements made for the different columns and the values obtained were compared to those predicted by different models.

4.4.1. Measurement of the eddy diffusion coefficient

The strategy used to measure the eddy diffusion term was described previously [21]. This term is given by the equation

$$h_{eddy} = h_{exp} - \frac{B}{\nu} - C_p\nu - C_f\nu \qquad (21)$$

where h_{exp} is the reduced HETP measured from the first and the second central moments of the peak, B is the longitudinal diffusion coefficient, derived from the results of the peak parking method (see previous section), C_p is the trans-particle mass transfer coefficient, derived from the combination of the results of the peak parking method, the equation of the EMT diffusion model for packed beds (which provides Ω), and Eq. (15) while C_f is the external film mass transfer coefficient, which is estimated from the correlation of Wilson & Geankoplis [22,23].

The accuracy of the experimental longitudinal diffusion term (B/ν) depends on two main errors: those made in estimating the slope of the plot of the peak variance versus the parking time and on the mean particle diameter used to calculate the reduced velocity. With highly diffusive compounds, the slope $(\Delta\sigma^2_{PP}/\Delta t_p)$ is measured with an error of less than a few percent and its precision is excellent with correlation coefficients of the linear regression being always larger than 0.999. As far as d_p is concerned, the SEM data provide accurate mean values, within a few percent if the instrument has been correctly calibrated. The errors made on the linear velocities (u_{PP} and u) are negligible with current HPLC pump systems (Agilent 1290 Infinity). Note that if the longitudinal diffusion term is preponderant at very low flow rates, it becomes marginal at flow rates close or larger than the optimal flow rate. Even a large error made on this term would have very little impact on the accuracy of the eddy diffusion data for high linear velocities.

The accuracy of the experimental trans-particle mass transfer term, $C_p\nu$, depends directly on the accuracy of the experimental parameter, Ω, which is measured with the peak parking experiments, assuming the parallel diffusion model in Eq. (12). The accuracy of this model is actually unknown. Alternate models have also been tested, such as the effective medium theory (EMT) model of diffusion in heterogeneous media in Eq. (13) [31]. It was shown that both the parallel and the EMT models provide similar and physically meaningful values for Ω. Eventually, the amplitude of the coefficient C_p is small (typically between 0.002 and 0.010 with shell particles), therefore, the overall $C_p\nu$ term is no larger than 0.15 within the range of reduced interstitial linear velocity used ($0 < \nu < 20$). Consequently, the experimental error made on the coefficient Ω has little repercussion on the accuracy of the experimental eddy diffusion term.

The error made on the external film mass transfer term derived from the Wilson & Geankoplis correlation is larger than the errors made on the (B/ν) and $C_p\nu$ terms. The validation of the correlation for totally porous particles assumed a constant value of the eddy diffusion term [23]. The experimental Sherwood number differed by 10–20% from the Sherwood number given by in references [22,23]. The Sherwood numbers measured for a homologous series of alkyl-benzene (toluene through butylbenzene) are typically equal to 7 for reduced velocities ν between 10 and 20. Consequently, C_f cannot exceed 0.030 but it is significantly larger than the C_p coefficient.

In conclusion, most of the error made on the measurement of the term $(B/\nu) + C_p\nu + C_f\nu$ arise from the last term, $C_f\nu$. For instance, for $\nu = 15$, the maximum experimental error made is of the order of $20\% \times 0.030 \times 15 = 0.09$. This is relatively small compared to the experimental overall reduced HETP, which is of the order of at least 1.5 for velocities above the optimum velocity.

This procedure was applied to data measured for the Atlantis (fully porous particles) and the Kinetex (shell particles) columns. Fig. 8A through D shows the results of these measurements for uracil, acetophenone, toluene, and naphthalene, respectively. At reduced linear velocities larger than 5, the eddy diffusion term of the Kinetex column is significantly smaller than that of the Atlantis column. On the average, the relative difference is −40%. Interestingly, as retention increases from uracil to naphthalene, this relative difference decreases to −28%. To a large extent, this result is explained by the A coefficient of the Atlantis column decreasing with increasing retention. As the residence time in the column increases, the radial concentration gradients caused by the radial distribution of the local external porosity (induced by the slurry packing process) are more effectively relaxed. This could be the reason why the trans-column velocity biases and the A term of

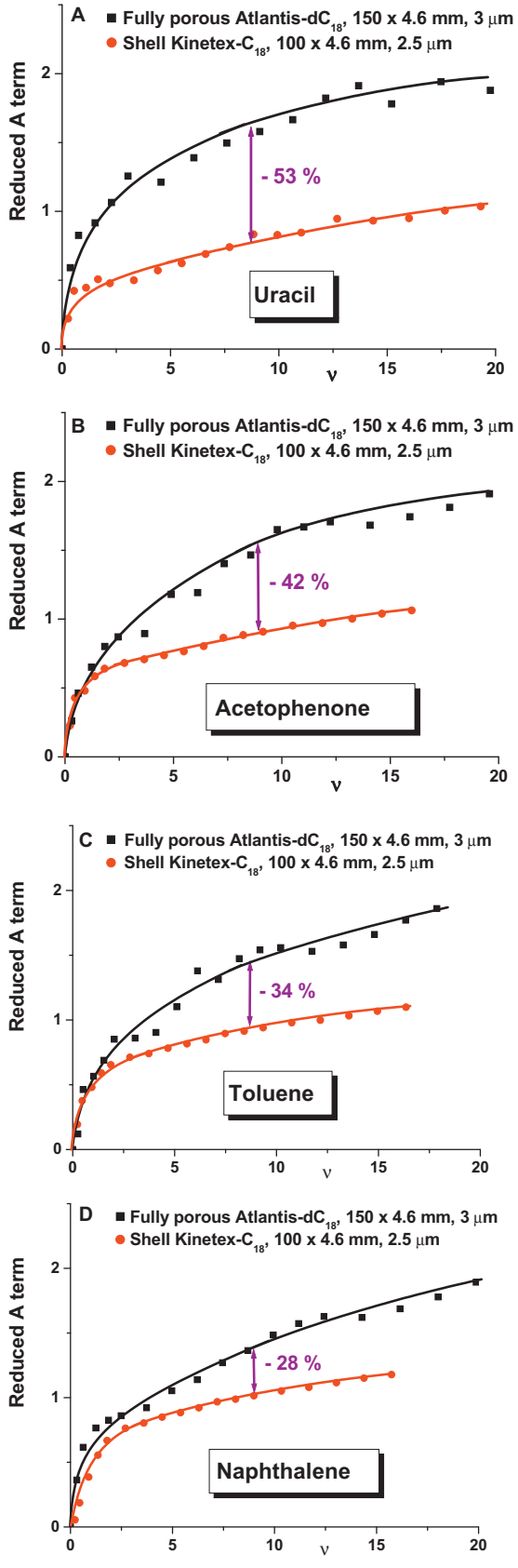

Fig. 8. Measurement of the eddy diffusion term by using the subtraction method (see details in the text) for a series of moderately retained compounds. Comparison between fully porous (Atlantis) and shell particles (Kinetex). (A) Uracil. (B) Acetophenone. (C) Toluene. (D) Naphthalene. Note the clearly smaller *A* term of columns packed with shell particles at reduced velocity around the minimum HETP and beyond.

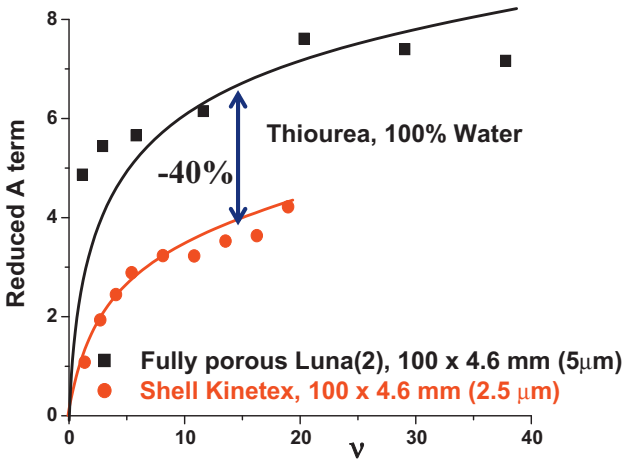

Fig. 9. Measurement of the eddy diffusion term by using the total pore blocking method (see details in the text) for the sample thiourea using pure water as the eluent. The mesopores were blocked with the liquid n-nonane. Comparison between fully porous (Luna) and shell particles (Kinetex). As in Fig. 8A–D, note the relatively smaller *A* term of columns packed with shell particles. Note also that the absolute values of the *A* term is much larger than that observed when the mesoporous volume is accessible to the sample.

columns packed with fully porous particles are larger than those of columns packed with shell particles.

These results were confirmed by measurements made with the pore blocking method. The HETPs of columns packed with shell and fully porous particles were measured before and after blocking the access of probe molecules to the mesopores by flushing the columns successively with liquid n-nonane and pure water. Since the probe compound used in these experiments should be insoluble in n-nonane, thiourea was used. The *A* coefficient is derived from these experimental data. Fig. 9 shows the results of these experiments for the Gemini (fully porous) and the Kinetex (shell) columns. For $\nu > 10$, the *A* coefficient of the latter column is about 40% smaller than that of the former. Yet the *A* values of the Kinetex column measured when access to the mesopores is not restricted are about half those when access is denied, which is due to the shorter residence time in the column, the smaller radial dispersion coefficient, and the role of the particle volume in the exchange of sample molecules between adjacent eluent stream-paths.

As a conclusion, we demonstrated that the high efficiencies of columns packed with sub-3 μm shell particles is due to an exceptionally low eddy diffusion term in their general van Deemter equation. We need now to analyze the reasons for this low value of the *A* coefficient of columns packed with shell particles. The eddy diffusion term of a packed bed is essentially controlled by the trans-channel velocity bias between adjacent particles (at a scale length of 1/6 th of the particle diameter or half the estimated inter-particle distance [36]), by the short-range inter-channel velocity bias (at the scale length of a few particle diameters), and by the trans-column velocity bias (at the scale length of the inner radius of the column tube).

4.4.2. *Trans-channel velocity bias*

The trans-channel eddy diffusion is *a priori* independent of whether the spherical particles are porous or not. The eluent velocity in the center of inter-particle stream-paths is always about twice the average linear velocity while the velocity at the wall of the particles is strictly zero (Hagen–Poiseuille law). According to the coupling theory of eddy diffusion developed by Giddings [36], this term is written:

$$h = \frac{0.01\nu}{1 + 0.03\nu} \tag{22}$$

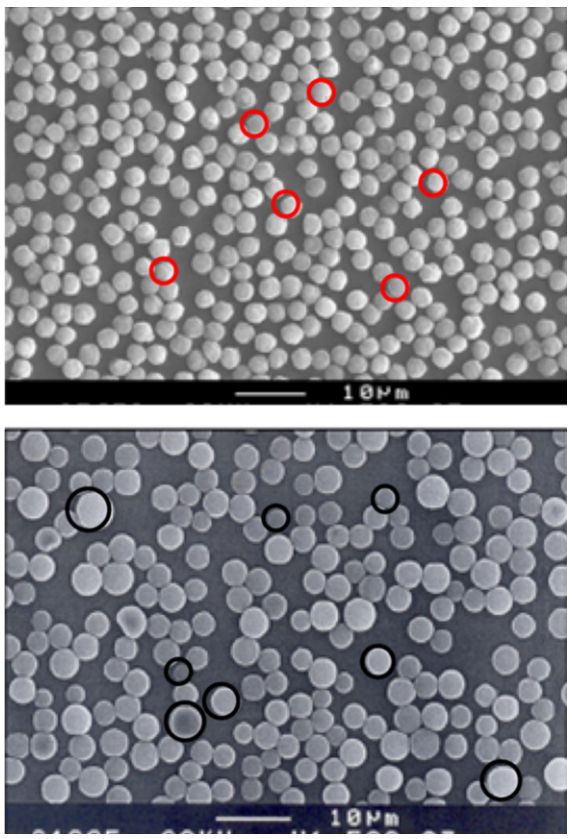

Fig. 10. SEM photographs of a large collection of 2.7 μm Halo 90 Å shell particles (A) and of 3.2 μm Symmetry 90 Å fully porous particles (B). Note the tighter size distribution of shell particles (relative standard deviation 5% *versus* 15%).

This equation shows that the transition linear velocity for trans-channel eddy diffusion is large ($\nu_{1/2} = 33$), suggesting that this term is nearly proportional to the linear velocity for small molecules ($h \simeq 0.01\nu$). At the minimum reduced HETP of columns packed with sub-3 μm particles ($\nu \simeq 7$), this term does not exceed 0.06. Clearly, it cannot account for the experimental differences mentioned above.

4.4.3. Inter-channel velocity bias

Short-range inter-channel velocity biases originate from differences in the interstitial linear velocity between neighbor stream-paths. Thus, this term depends on the degree of heterogeneity of the channels between neighbor particles. The size distributions of shell particles are narrow (the relative standard deviation of their distribution is around 5% [13,14]) while that of fully porous particles is around 15–20%). It could be expected that columns packed with shell particles would be more homogeneous than those packed with fully porous ones. Fig. 10A and B shows scanning electron microscopy (SEM) photographs of a collection of about 200 particles of Halo (A, shell particles) and Luna (B, fully porous particles), respectively. The tight PSD of the Halo particles is directly related to the tight PSD of their 1.7 μm solid cores [14]. The fabrication of the 0.5 μm porous layers is reproducible for all the particles and does not affect the width of the PSD of the final shell particles. Yet, this does not warrant that the consolidated beds obtained by slurry packing have a highly homogeneous structure at the scale of a few particle diameters. The presence of local defaults and other heterogeneities can cause the formation of wide or narrow inter-particle channels, increasing the short-range inter-channel velocity biases. Thus, the consequences of these short-range fluctuations of the dimensions of the inter-particle channels across the packed bed is still unclear. A previous detailed study of their performance gave different conclusions regarding the bed behavior of Kinetex and Halo shell particles. Beds of the former particles have a smaller short-range inter-channel eddy diffusion term than columns packed with fully porous particles whereas no significant difference was observed for beds of the latter particles. Recent simulation studies performed by random reconstruction of packed beds made of particles having wide or narrow particle size distributions show no significant difference in their resulting short-range eddy diffusion term [37].

Most likely, the short-range inter-channel velocity biases are likely not responsible for the difference between the *A* terms of columns packed with shell and fully porous particles.

4.4.4. Trans-column velocity bias

The trans-channel velocity biases result from the consolidation of the packed bed during the slurry packing process. Because the stress applied to particles is larger near the wall than in the column center, the local external porosity tends to be slightly smaller close to the wall than in the column center [38], causing the column permeability to vary across the column. The linear mobile phase velocity is typically 2% higher in the center of columns packed with fully porous particles than close to its wall [39]. These considerations suggest a simple model explaining the origin of trans-column velocity bias in packed columns. The smoother the external surface of the particles, the smaller the shear stress between particles in direct contact during the slurry packing process. The relative displacements of particles during bed consolidation are larger, hence the distribution of strains across the column is wider, causing a wider distribution of the local permeability and a lower total column permeability. The external porosity of the column packed with smooth, fully porous Luna particles (see Fig. 11A) measured by inverse size exclusion chromatography (ISEC) is 0.37. The local external porosity is heterogeneous and its radial distribution can be estimated using local electrochemical detection [39]. In contrast, the external surface of shell particles is rugged (see Fig. 11B). The shear stress in between shell particles in contact is larger than between smooth particles. The strain taking place during bed consolidation is smaller and the packed bed is less densely packed. This was confirmed from ISEC measurements, which give an average external porosity around 0.41. Furthermore, the external porosity is radially more uniform and the trans-column velocity bias reduced.

This model is validated for the Halo column [14]. The relative velocity difference between the center and the wall regions of this column is only 0.7%. In contrast, no significant difference was found between the Kinetex (1.7%) and the Luna (2%) columns.

4.4.5. On the origins of the eddy diffusion term

We demonstrated that the *A* term of the 4.6 mm I.D. columns packed with shell particles is smaller than that of the columns packed with fully porous particles. Yet, the interpretation of this observation remains arguable. Different conclusions can be drawn from the data measured with the Kinetex column (reduction of the short-range inter-channel velocity bias) and with the Halo column (reduction of the trans-column velocity bias). This suggests that more studies, particularly studies involving the reconstruction of the actual morphology of packed beds [40], the calculation of the local flow velocity profile across this reconstructed structure, and of the convective-diffusive transport process [41] are definitively necessary. At the same time, rheological measurements are needed to measure the shear stress between rugged and smooth particles to check if the trans-column mass transfer term is smaller with shell than with fully porous particles.

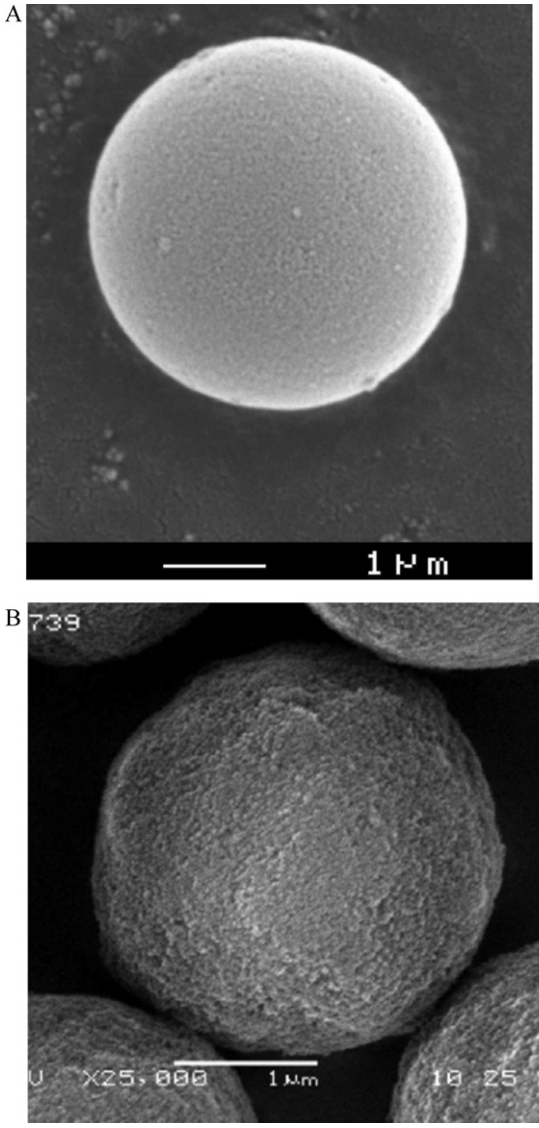

Fig. 11. SEM photographs of the external surface area of a single 3.5 μm Luna fully porous particle (A) and of a 2.7 μm Halo 90 Å shell particles (B). Note the relatively enhanced ruggedness of shell particles with respect to the fully porous particles.

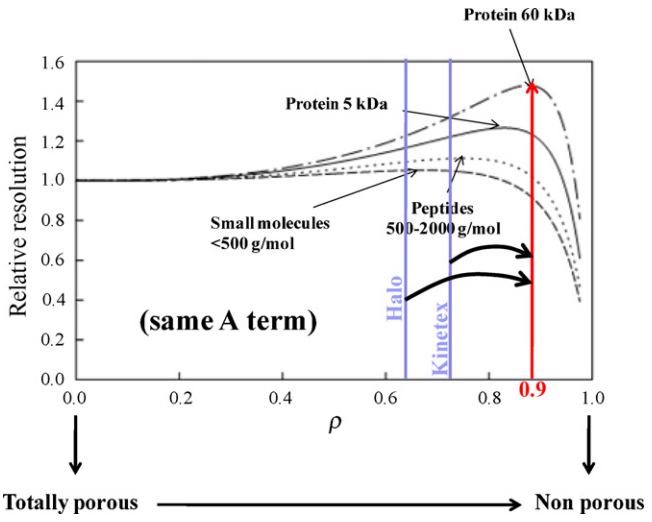

Fig. 12. Ratio of the theoretical peak resolution with columns packed with shell particles to that of columns packed with fully porous particles as a function of the parameter ρ. In the calculation, the velocity was fixed at four times the optimal velocity, the Henry's constants of the pair of compounds was set at $K_{shell,1} = 3.5$ and $K_{shell,2} = 4.0$, the same A term was assumed for both types of particles, and the external film mass transfer coefficient was estimated from the Wilson & Geankoplis correlation. Note the negligible impact of the shorter diffusion path for the resolution of small molecules and the desired range $0.8 < \rho < 0.9$ for the optimum resolution of large proteins.

4.5. Improvement of the kinetic performance of shell particles

The exceptional performance of columns packed with shell particles is explained by the B and A terms of their van Deemter equations being smaller than those of columns packed with fully porous particles. The contribution of a decrease of their C_p coefficients (due to the shorter diffusion path across these particles) to the enhanced performance of these columns is negligible because already the C_p coefficient of fully porous particles is small with respect to the experimental C coefficient anyway. By combining Eq. (15), the results of the peak parking experiments, and the EMT diffusion model to estimate the coefficient Ω, we can determine values of the average C_p coefficients. The values obtained are 0.0078 for the Atlantis ($\rho = 0$), 0.0047 for the Halo 90 ($\rho = 0.63$), 0.0040 for the Halo 160 ($\rho = 0.63$), and 0.0023 for the Kinetex ($\rho = 0.72$) columns. Therefore, at a reduced velocity of $\nu = 8$, close to the optimum velocity, the reduced HETPs of the columns packed with shell particles due to their faster trans-particle diffusivity are smaller than those of the Atlantis column packed with fully porous particles. The differences in $C_p\nu$ are 0.03 (Halo 90), 0.04 (Halo 160), and 0.05 (Kinetex). For the sake of comparison, the decreases in the axial diffusion term (B/ν) for moderately retained compound are 0.12 (Halo 90), 0.13 (Halo 160), and 0.20 (Kinetex). The decreases in the eddy diffusion terms (A) are 0.11 (Halo 90), 0.31 (Halo 160), and 0.29 (Kinetex). Accordingly, improving the C_p coefficients by increasing the structural parameter ρ is clearly useless for small molecules [42]. It would be more important to keep constant the porous shell thickness than to use weak eluents in order to avoid column overloading and peak tailing.

This conclusion, however, does not apply to large molecules such as proteins because their diffusion in porous shells is significantly hindered and slower than that of small molecules. The relative resolution (defined as the ratio of the peak resolution obtained for shell particles characterised by a parameter $0 < \rho < 1$ to that of the same but fully porous particles, e.g. $\rho = 0$) on columns packed with shell and fully porous particles for compounds having different molecular sizes (small molecules, peptides, small protein, and large protein) is plotted in Fig. 12 as a function of the parameter ρ. In this figure, the linear velocity was fixed at four times the optimal velocity. This figure shows that the optimum peak resolution of proteins is achieved for $0.8 < \rho < 0.9$. All the necessary information regarding the model of mass transfer is given in Ref. [42]. The fundamental equation was assumed to be Eq. (1).

In conclusion, if the molecular diffusivity in the porous shell is the limiting kinetic factor, decreasing the relative thickness of the shell could improve resolution between the peaks of large molecules. Yet, the former shell particles, which had values of ρ between 0.8 and 0.9 (e.g., the 55 μm Zipax and the 5 μm Poroshell) were not as successful as current shell particles because (1) their loading capacity was low and (2) their minimum reduced HETP was larger than 2 (most likely because the porosity of particles affects the A term of the columns packed with them [32,43]).

In fact, the molecular diffusivity of large molecules through the porous shell does not control the solid–liquid mass transfer ($C\nu$) term. By combining the measurements of the reduced HETP and the results of peak parking experiments made with insulin and with the first generation of Halo shell particle (90 Å), we found that the C_p coefficient (0.020) of these earlier columns was much smaller than their overall C term (0.295) [14,18]. The apparent rate con-

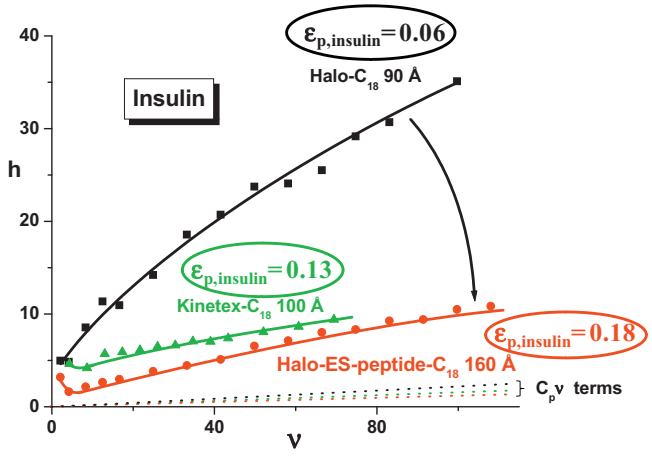

Fig. 13. Plots of the reduced plate heights of insulin (symbols and thick solid lines) measured with three columns packed with shell particles. The dotted lines account for the sole trans-particle mass transfer resistance term. Note that the solid–liquid mass transfer resistance of insulin is controlled by the external film mass transfer resistance, which decreases when increasing the porosity of the particle accessible to the protein.

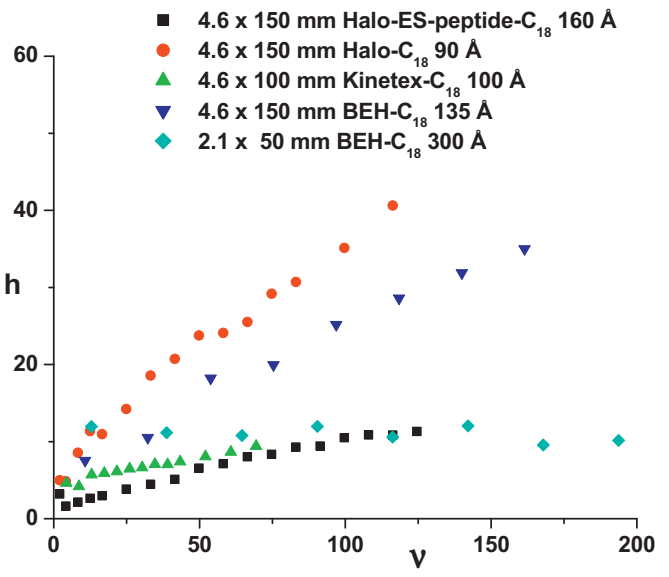

Fig. 14. Plots of the reduced plate heights of insulin measured with fully porous particles (1.7 μm BEH-C_{18} 135 Å and 300 Å). Note the faster external film mass transfer with the large average mesopore size.

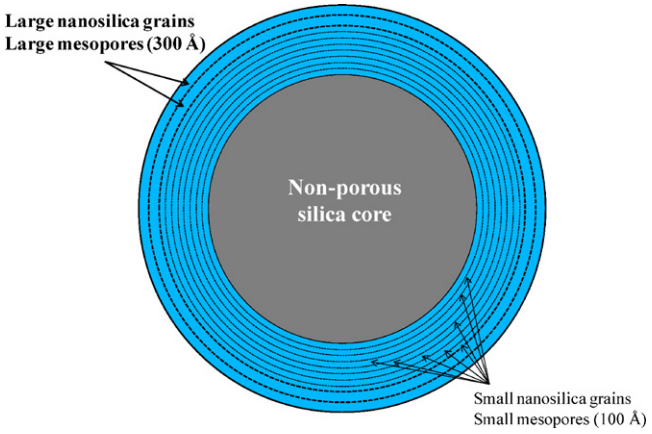

Fig. 15. Anticipated structure of future silica particles for application in HPLC. Presence of solid non-porous core to allow the controlled step-by-step building of a thick porous layer. The very first layers (8 first layers in this graph) are prepared with thin nano-grains of silica to generate a high loading capacity (important for small molecules). The last two layers (or possibly the last one) are prepared with larger nano-grains of silica to allow the easy access to the porous layer (important for large molecules).

stant of insulin diffusion through the shell appears then to be 15 times larger than that of its diffusion into the stagnant mobile phase impregnating the particle pores from the mobile phase percolating through the bed. The particle–liquid mass transfer resistance is then controlled by the external film mass transfer. The slow rate of transfer of large molecules such as proteins from the moving into the stagnant eluent is not related to an unlikely excessive thickness of an immobile film of eluent around the particles but to the probability for a molecule to find a pore opening in the particle surface and enter into the pore. This probability depends directly on the porosity of the particle that is accessible to the protein at its external surface. Fig. 13 shows that the value of the *C* coefficient does not depend on the average mesopore size of the porous shell. The Kinetex and Halo 90 particles have the same average pore size, yet, Kinetex columns have a flatter *C* branch. The *C* coefficient depends on the fraction of the external surface area of the particle which is open for access by the protein. This fraction could be adjusted by modifying, if possible, the size distribution of the pore openings (by having wider and/or larger average sizes and/or shorter alkyl bonded chains). The higher efficiency of the Halo 160 column is certainly explained by a decrease in the k_{ext} coefficient, probably due to an increase in the total surface area of the pore openings.

Fig. 14 compares the reduced HETP plots of insulin measured on the columns packed with the three brands of shell particles (the Halo 90 and 160, and the Kinetex columns) and those of columns packed with two brands of sub-2 μm fully porous particles (BEH-C_{18}), which have small and large average mesopore sizes (130 and 300 Å). The *C* branch of the column packed with the particles having the larger pores is significantly flatter, probably because the access to the porous particles is easier with larger pores (although an average pore size of 130 Å should be sufficiently large to permit access of the molecules). The comparison of the curves for the two Halo columns, the Kinetex, and the BEH-C_{18} 130 Å columns demonstrate that it is not the average pore size alone that controls mass transfer kinetics in HPLC columns.

Therefore, in order to obtain columns packed with shell particles that have a sufficiently large loading capacity for most analytical applications, we need that these particles have (1) a relatively thick porous shell; with (2) a proper average mesopore size compared to the size of the analytes; and (3) that the access of sample molecules to the mesopore volume be easy. It seems probable that access of molecules to the porous shell would be facilitated by preparing shells having a radial gradient of porosity and pore size, with one or a few external layers of higher porosity and average pore size than the bulk of the shells. Fig. 15 illustrates a shell structure that could provide excellent resolution for small and large molecules and an acceptable loading capacity.

5. Conclusion

The results of our work demonstrate that the very high efficiency of columns packed with the new sub-3 μm shell particles (Halo 90 and 160, Kinetex, Poroshell120, and now Eiroshell [37]) for small molecules is essentially due to the combination of a smaller longitudinal diffusion coefficient and a lower eddy diffusion coefficient (respectively 10 and 30% lower than for columns packed with fully porous particles). It remains unknown whether the lower *A* term of the van Deemter equation is due to a decrease of either the short-range inter-channel or of the trans-column velocity biases in these

4.6 mm I.D. columns. To elucidate this question, investigations should be pursued in two different directions: (1) the reconstruction by confocal laser scanning microscopy of the structure of actual beds of shell particles consolidated in thin glass capillary tubes; the calculation of the flow velocity field in these columns, coupled with a convective-diffusive mass transport model should shed light on the importance of short-range and trans-capillary velocity bias [37]. (2) Rheological measurements of the shear stresses between shell particles or fully porous particles in packed beds and of the friction coefficients between these particles or between their beds and the column tube will inform on the degree of strain taking place during bed consolidation [38].

The most important conclusion of this work is that, in contrast with conventional wisdom, the trans-particle mass transfer resistance coefficient of chromatographic columns for compounds of molecular weight below ca. 1000 Da is small or negligible, whether the column is packed with shell or with fully porous particles. Results of the peak parking method show that the sample diffusivity across the porous shell does not affect significantly the overall C coefficient of molecules as large as insulin, which remains controlled by the external film mass transfer resistance. This resistance depends essentially on the accessibility of the mesopore network through the openings of the pores on the external surface of the shells.

Therefore, improvements of the mass transfer kinetics of large-size molecules through columns packed with shell particles could be obtained by making more accessible the superficial layer of the porous shell, the layer in direct contact with the percolating eluent. This first layer should have larger mesopores (ca. 300 Å) and/or shorter alkyl bonded chains (e.g., C_4). In order to maintain an acceptable column loading capacity for small proteins, the average mesopore size of the underlying layers could be kept around 100 Å.

In conclusion, we suggest that scientists who know how to prepare standard shell or fully porous particles try and build around them a layer (like a crust) made of a few layers of porous silica with a markedly larger porosity than the underlying porous silica. If they succeed these new, sophisticated particles, once properly packed, should provide columns exhibiting a very high efficiency for large molecules, due to faster external film mass transfers. We hope to have the opportunity to assess the kinetic performance of such new packing materials in the near future.

Nomenclature

Roman letters

a	EMT parameter defined in Eq. (13)
$A(\nu)$	eddy diffusion term in the reduced van Deemter equation (1)
B	longitudinal diffusion coefficient in the reduced van Deemter equation (1)
$C(t)$	concentration profile ($kg\,m^{-3}$)
C	overall experimental solid–liquid mass transfer coefficient
C_p	trans-particle mass transfer coefficient in the reduced van Deemter equation (1)
$C_{p,shell}$	trans-particle mass transfer coefficient in the reduced van Deemter equation (1) for shell particles
$C_{p,fullyporous}$	trans-particle mass transfer coefficient in the reduced van Deemter equation (1) for fully porous particles
C_f	external film mass transfer coefficient in the reduced van Deemter equation (1)
D_1	sample diffusion coefficient in homogeneous medium 1 (m^2/s)
D_2	sample diffusion coefficient in homogeneous medium 2 (m^2/s)
D_p	sample diffusivity coefficient through the particle volume (m^2/s)
d_p	average particle size (m)
D_{eff}	effective diffusion coefficient in the porous shell (m^2/s)
D_m	bulk molecular diffusion coefficient (m^2/s)
F_v	inlet flow rate (m^3/s)
H	plate height (m)
h	total reduced column HETP
h_{exp}	experimental reduced HETP
h_{eddy}	eddy diffusion reduced HETP term
h_{Film}	external film mass transfer reduced HETP term
h_{Heat}	additional reduced HETP generated by frictional heating in the column
k_1	zone retention factor
K_{shell}	distribution coefficient between the eluent volume and the solid porous medium
L	column length (m)
P_f	power heat friction (W/m)
ΔP	column pressure drop (Pa)
R_c	column inner radius (m)
Sh	Sherwood number
t	time (s)
T	temperature (K)
t_p	parking time (s)
u	interstitial linear velocity (m/s)
u_{PP}	migration linear velocity in the peak parking method (m/s)

Greek letters

ϵ_e	external column porosity
$\epsilon_{shell,p}$	porosity of the shell accessible to the sample molecule
γ_e	external obstruction factor
λ	eddy diffusion parameter associated with a flow exchange mechanism
μ_1	first moment (s)
$\mu_2^{'}$	second central moment (s^2)
$\mu_{1,ex}$	first moment of the extra-column band profiles (s)
$\mu_{2,ex}^{'}$	second central moment of the extra-column band profiles (s^2)
ν	reduced interstitial linear velocity of the eluent to the particle diameter d_p and bulk molecular diffusion coefficient D_m
ω	eddy diffusion parameter associated with a diffusion exchange mechanism
Ω	ratio of the intra-particle diffusivity of the sample through the porous shell to the bulk diffusion coefficient
ρ	ratio of the diameter of the solid core to that of the core–shell particle
σ_{PP}^2	Variance of the eluted peak in the peak parking experiment (s^2)

Acknowledgements

This work was supported in part by grant CHE-06-08659 of the National Science Foundation and by the cooperative agreement between the University of Tennessee and the Oak Ridge National Laboratory. We thank Jack Kirkland and Joseph DiStefano (Advanced Material Technologies, Wilmington, DE, USA) for the generous gifts of Halo-C_{18} 160 Å columns, Tivadar Farkas (Phenomenex, Torrance, CA, USA) for those of Kinetex columns, Uwe Neue (Waters, Milford, MA) for those of narrow bore columns packed with sub-2 μm BEH particles, and Ron Majors (Agilent Technologies, Little Falls) for the gift of the last flask

of Zipax packing material and of Poroshell columns to be tried soon.

References

[1] C. Horváth, B.A. Preiss, S.R. Lipsky, Anal. Chem. 39 (1967) 1422.
[2] C. Horváth, S.R. Lipsky, J. Chromatogr. Sci. 7 (1969) 109.
[3] K. Kaczmarski, G. Guiochon, Anal. Chem. 79 (2007) 4648.
[4] J.F.K. Huber, J. Chromatogr. Sci. 9 (1971) 72.
[5] J.F.K. Huber, C.A.M. Meijers, J.A.R. Hulsman, Anal. Chem. 44 (1972) 111.
[6] I. Halasz, H. Englehardt, J. Asshauer, B.L. Karger, Anal. Chem. 42 (1970) 1460.
[7] B.L. Karger, L.V. Berry, Clin. Chem. 17 (1971) 757.
[8] J.J. Kirkland, Anal. Chem. 43 (1971) 36A.
[9] J.J. Kirkland, Anal. Chem. 41 (1969) 218.
[10] J.J. Kirkland, Anal. Chem. 64 (1992) 1239.
[11] X. Wang, W.E. Barber, P.W. Carr, J. Chromatogr. A 1107 (2006) 139.
[12] J.J. DeStefano, T.J. Langlois, J.J. Kirkland, J. Chromatogr. Sci. 46 (2008) 254.
[13] F. Gritti, G. Guiochon, J. Chromatogr. A 1157 (2007) 289.
[14] F. Gritti, I. Leonardis, J. Abia, G. Guiochon, J. Chromatogr. A 1217 (2010) 3219.
[15] F. Gritti, I. Leonardis, D. Shock, P. Stevenson, A. Shalliker, G. Guiochon, J. Chromatogr. A 1217 (2010) 1589.
[16] E. Olh, S. Fekete, J. Fekete, K. Ganzler, J. Chromatogr. A 1217 (2010) 3642.
[17] F. Gritti, G. Guiochon, J. Chromatogr. A 1217 (2010) 1604.
[18] F. Gritti, G. Guiochon, J. Chromatogr. A, in press, JCA-10-1136.
[19] F. Gritti, G. Guiochon, Chem. Eng. Sci. 61 (2006) 7636.
[20] K. Miyabe, G. Matsumoto, Y. Guiochon, Anal. Chem. 79 (2007) 1970.
[21] F. Gritti, G. Guiochon, J. Chromatogr. A 1217 (2010) 5137.
[22] E. Wilson, C. Geankoplis, J. Ind. Eng. Chem. Fundam. 5 (1966) 9.
[23] K. Miyabe, Y. Kawaguchi, G. Guiochon, J. Chromatogr. A 1217 (2010) 3053.
[24] F. Gritti, M. Martin, G. Guiochon, Anal. Chem. 81 (2009) 3365.
[25] F. Gritti, G. Guiochon, Anal. Chem. 81 (2009) 2723.
[26] F. Gritti, G. Guiochon, J. Chromatogr. A 1217 (2010) 5069.
[27] K. Kaczmarski, F. Gritti, J. Kostka, G. Guiochon, J. Chromatogr. A 1216 (2009) 6575.
[28] F. Gritti, G. Guiochon, J. Chromatogr. A 1216 (2009) 1353.
[29] F. Gritti, C. Sanchez, T. Farkas, G. Guiochon, J. Chromatogr. A 1217 (2010) 3000.
[30] G. Guiochon, A. Felinger, A. Katti, D. Shirazi, Fundamentals of Preparaative and Nonlinear Chromatography, 2nd ed., Academic Press, Boston, MA, 2006.
[31] F. Gritti, G. Guiochon, AIChE J. (2010).
[32] F. Gritti, G. Guiochon, AIChE J. (2010).
[33] R. Landauer, J. Appl. Phys. 23 (1952) 779.
[34] H. Davis, J. Am. Ceram. Soc. 60 (1977) 499.
[35] F. Gritti, G. Guiochon, Anal. Chem. 78 (2006) 5329.
[36] J. Giddings, Dynamics of Chromatography, Marcel Dekker, New York, NY, 1965, p. 1217.
[37] 35th International Symposium on High Performance Liquid Phase Separations & Related Techniques, June 2010.
[38] B.G. Yew, J. Ureta, R.A. Shalliker, E.C. Drumm, G. Guiochon, AIChE J. 49 (2003) 642.
[39] J. Abia, K. Mriziq, G. Guiochon, J. Chromatogr. A 1216 (2009) 3185.
[40] D. Hlushkou, S. Bruns, U. Tallarek, J. Chromatogr. A 1217 (2010) 3674.
[41] S. Khirevich, A. Daneyko, A. Holtzel, A., S.-M.A., U. Tallarek, J. Chromatogr. A. 1217 (2010) 4713.
[42] K. Horvath, F. Gritti, J. Fairchild, G. Guiochon, J. Chromatogr. A (2010).
[43] F. Gritti, G. Guiochon, AIChE J. 56 (2010) 1495.